JVST B
Journal of Vacuum Science & Technology B

Selective lateral photoelectrochemical wet etching of InGaN nanorods

Cite as: J. Vac. Sci. Technol. B **38**, 060602 (2020); https://doi.org/10.1116/6.0000527
Submitted: 06 August 2020 . Accepted: 18 September 2020 . Published Online: 07 October 2020

Chunyu Zhao, Xu Zhang, Chak Wah Tang, Jiannong Wang, and Kei May Lau

JVST B
Journal of Vacuum Science & Technology B

LETTER

avs.scitation.org/journal/jvb

Selective lateral photoelectrochemical wet etching of InGaN nanorods

Cite as: J. Vac. Sci. Technol. B 38, 060602 (2020); doi: 10.1116/6.0000527
Submitted: 6 August 2020 · Accepted: 18 September 2020 ·
Published Online: 7 October 2020

Chunyu Zhao,[1,2] Xu Zhang,[1] Chak Wah Tang,[1] Jiannong Wang,[2] and Kei May Lau[1,a)]

AFFILIATIONS

[1]Department of Electronic and Computer Engineering, Hong Kong University of Science and Technology, Clear Water Bay, Kowloon, Hong Kong
[2]Department of Physics, Hong Kong University of Science and Technology, Clear Water Bay, Kowloon, Hong Kong

[a)]**Electronic mail:** eekmlau@ust.hk

ABSTRACT

Vertically aligned InGaN nanorods (NRs) sandwiched between GaN layers on sapphire substrates were synthesized by photoelectrochemical (PEC) wet etching. The In_xGaN/In_yGaN superlattice layer was laterally etched into NRs by selectively removing the material between dislocations due to the nonradiative recombination occurring at the dislocations. The mechanism of this PEC etching is examined in detail by characterizing it with different InGaN doping concentrations, KOH concentrations, and etching times. A lateral etch rate of 80 nm/min was achieved for an n-type doping concentration of 1.1×10^{19} cm^{-3} and a KOH concentration of 2.2M. This demonstration provides a simple but promising method for GaN nanostructure fabrication, which suggests further potential applications for GaN-based optical devices.

I. INTRODUCTION

Improving the performance of GaN-based light emitting diodes (LEDs) has attracted interest because of their wide application as solid-state lighting sources.[1,2] Conventional LEDs have a low light extraction efficiency, with only around 6% of the light emitted into the free space for the current planar-architecture LEDs.[3] GaN-based nanostructures, featuring a superior high surface area to volume ratio, have been widely used to enhance the light extraction of such LEDs.[4,5] Generally, two major types of methods, bottom-up and top-down techniques, have been used to fabricate nanostructures. In the bottom-up methods, III-nitride nanostructures have been grown by molecular beam epitaxy (MBE) and metal-organic chemical vapor deposition (MOCVD) through selective-area growth,[6,7] catalyst-assisted growth,[8,9] and self-assembled growth.[10,11] However, all these bottom-up growth methods require precise control of the complicated growth conditions while introducing growth defects such as stacking faults or inversion domain boundaries.[12–15]

The alternative top-down methods, meanwhile, provide a flexible route for the fabrication of GaN nanostructures from normal thin films by dry etching.[16–18] However, plasma dry etching presents some significant challenges. First, it is difficult to achieve well-controlled features with vertical sidewalls and high-aspect-ratio nanostructures due to the slight lateral etching.[19] Second, the ion bombardment in the plasma dry etching may damage the crystalline quality of the material and deteriorate device performance.[20] Combining the dry etching technique with wet chemical etching, a simple method that demonstrates advantages such as low cost, high selectivity, and a smooth surface without damage, enables the fabrication of nanostructures with excellent uniformity and optical quality.[21–24] The wet etch solution which has been widely applied to III-nitrides is potassium hydroxide (KOH).[25] Highly sensitive etching of N-face GaN in the hydroxide ions (OH^-) in KOH solutions will produce surface texturing on the side walls or leave triangular etched pits on the m-plane surface.[26,27] Therefore, KOH wet etching can also be used to estimate the threading dislocation densities in GaN.[28]

An enhanced wet etching technique, photoelectrochemical (PEC) etching, has recently attracted considerable attention due to its excellent bandgap selectivity. PEC etching is a light-induced material etching technique that utilizes photogenerated holes to oxidize and decompose the n-GaN in an electrolyte. During the PEC etching, a high-power ultraviolet (UV) lamp is used to illuminate the material with the above-bandgap light to generate sufficient electron-hole pairs. PEC etching of n-type GaN layers was first reported by Minsky *et al.* in 1996.[29] GaN cantilevers with

lengths beyond 100 μm were later achieved using PEC etching to form deep undercut structures.[30] Highly efficient InGaN microcavity LEDs incorporating a high index contrast air gap distributed Bragg reflector (DBR) were realized using PEC to selectively etch GaN/AlGaN layers to Air/AlGaN layers,[31] while a 5-μm-thick GaN epitaxial film was successfully lifted off from a 4-in. sapphire substrate by PEC selective lateral etching of the InGaN release layer through cross-shaped perforations.[32] Recently, an ultralow-threshold InGaN/GaN quantum dot microring laser was demonstrated, in which an air gap providing optical isolation was selectively etched by PEC.[33]

Despite these intensive studies, the investigation of selective lateral etching to reshape In_xGaN/In_yGaN superlattice sacrificial layers (SSLs) into nanorods (NRs) has not been reported before. In this work, for the first time, we demonstrate InGaN/GaN nanostructures with InGaN NRs sandwiched between GaN layers using PEC etching. Furthermore, various etching conditions are investigated, and the corresponding PEC etching mechanism is also illustrated. This cost-effective PEC etching process holds significant implications for the realization of a broad range of nano-optoelectronic devices in the future.

II. EXPERIMENTS

The InGaN/GaN epilayers were grown on a 2-in. c-plane sapphire substrate by MOCVD. The epitaxial structure includes 3-μm-thick silicon-doped n-type GaN, five pairs of 20 nm/20 nm n-type In_xGaN/In_yGaN ($x = 0.09$, $y = 0.11$) SSLs, a 20-nm $Al_{0.2}Ga_{0.8}N$ etching stop layer, and a 200-nm undoped GaN layer on top, as shown in Fig. 1(a). The etching stop layer was used to prevent vertical etching into the top GaN layer.

The fabrication steps are illustrated as follows: First, 50-nm-thick chromium circular patterns with a diameter of 5 μm were evaporated on the GaN surface to serve as a dry etching mask [Fig. 1(b)]. To get a microdisk structure, the GaN epilayers were etched down to the n-type GaN layer by the inductively coupled plasma (ICP) etching process, with In_xGaN/In_yGaN SSL sidewalls exposed [Fig. 1(c)]. Afterward, a bilayer of Ti/Au (5/50 nm) was deposited by the electron beam evaporation process on the n-type GaN layer as a cathode [Fig. 1(d)], where the photogenerated electrons will accumulate during PEC etching. The PEC wet etching was carried out in the KOH solution at room temperature for the selective lateral etching process [Fig. 1(e)]. A 300 W Xe lamp was used as the illumination source to generate electron-hole pairs in the material. No electrical bias or stirring was applied during etching. The influences of different etching times and KOH concentrations in the PEC etching were investigated.

The electron concentration and resistivity of the n-type In_xGaN/In_yGaN SSLs were identified by the Hall effect measurement of the as-grown n-type InGaN thin film, which was characterized by the Hall system (Ecopia HMS-5500) under a magnetic field of 0.55 T. Samples A, B, and C featured the same structure as mentioned above, except that the n-type In_xGaN/In_yGaN SSLs had different SiH_4 flow rates of 6, 12, and 16 SCCM, respectively. The morphologies of samples A, B, and C after etching were systematically investigated as a function of the n-type In_xGaN/In_yGaN SSL doping concentration. Furthermore, the PEC etching of sample C was investigated using different etching times from 10 to 30 min and different KOH concentrations from 0.04 to 2.2M. The NR structure of the In_xGaN/In_yGaN SSLs after etching was studied by scanning electron microscopy (SEM, JEOL-7100F) and dual-beam focused ion beam scanning electron microscopy (FIB-SEM, FEI Helios G4 UX).

III. RESULTS AND DISCUSSION

With the lower resistivity of InGaN SSLs, more electron-hole pairs should be easily generated and separated, resulting in an enhanced PEC etching. To confirm this assumption, several groups of n-type InGaN thin films were grown with different electron concentrations, by varying the SiH_4 flow rate. The electron concentration and resistivity as a function of the SiH_4 flow rate for the as-grown n-type InGaN thin films were characterized by the Hall system at room temperature. As shown in Fig. 2, the InGaN thin

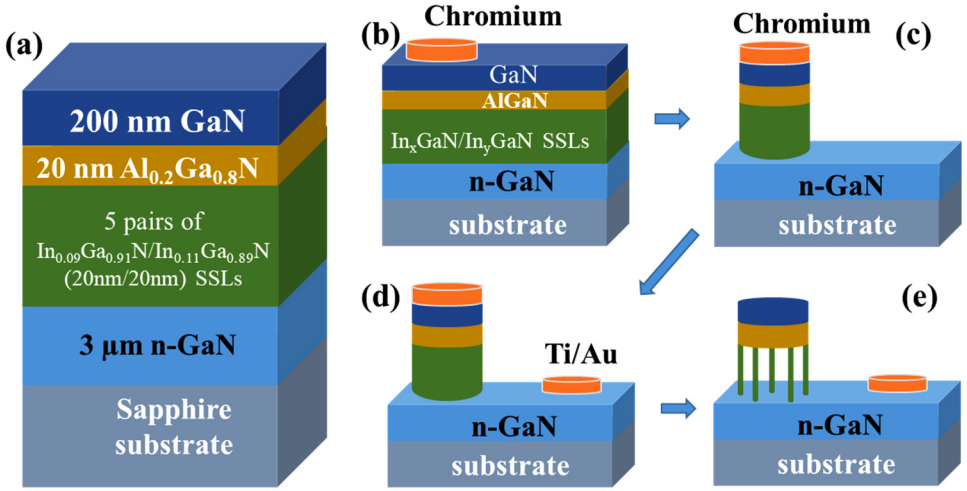

FIG. 1. Schematic diagram illustrating the process flow: (a) epitaxial growth of In_xGaN/In_yGaN SSLs sandwiched between GaN. (b) Chromium deposition as an etching mask. (c) GaN disk formed by ICP etching. (d) Ti/Au cathode deposition. (e) PEC etching, forming a nanorod structure sandwiched by GaN.

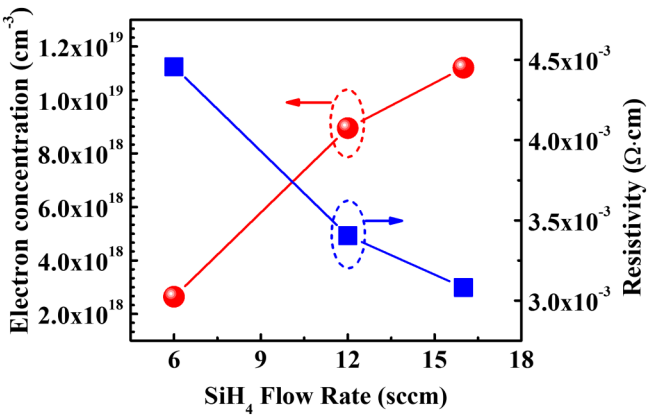

FIG. 2. Effect of SiH_4 flow rate on the electron concentration and resistivity of n-type InGaN thin films.

film grown under a SiH_4 flow rate of 6 SCCM gives a high resistivity of $4.5 \times 10^{-3}\,\Omega$ cm and a low electron concentration of 2.6×10^{18} cm^{-3}. The increase in SiH_4 flow rate from 6 to 12 SCCM leads to an electron concentration increase to 8.9×10^{18} cm^{-3} and a resistivity decrease to $3.4 \times 10^{-3}\,\Omega$ cm. When the SiH_4 flow rate reaches 16 SCCM, the electron concentration and resistivity change almost linearly and have a maximum value of 1.1×10^{19} cm^{-3} and a minimum value of $3 \times 10^{-3}\,\Omega$ cm, respectively.

Figure 3 illustrates the cross-sectional SEM images of samples A, B, and C after a 10-min PEC etching process in 2.2M KOH. The Ti/Au cathode is located adjacent to the microdisk to make a shorter collection path for the electrons, as shown in the low-magnification SEM images in Figs. 3(a)–3(c). An obvious morphology of the n-type In_xGaN/In_yGaN SSL etching and alignment evolution as a dependence of the SiH_4 flow rate can be observed, suggesting that the electron concentration of the n-type In_xGaN/In_yGaN SSLs plays a crucial role in the PEC etching process. As indicated in Fig. 3(a), no NRs form for sample A, in which the electron concentration is 2.6×10^{18} cm^{-3}. The corresponding zoomed-in SEM image in Fig. 3(d) confirms that only some black-colored areas associated with the incipient NR formation can be observed at the In_xGaN/In_yGaN SSL region, indicating that the PEC etching rate is very slow in this situation. Compared to sample A, the slightly increased electron concentrations of sample B mean that a clear indication of etching-hole-isolated NRs can be found in the In_xGaN/In_yGaN SSL region of the whole disk, as shown in Fig. 3(b). As indicated in the zoomed-in SEM image of sample B shown in Fig. 3(e), only a small number of etching holes can be found with a diameter in the range of 5–50 nm. Furthermore, with the even higher electron concentration in sample C, etching is further enhanced. As shown in Fig. 3(f), the diameters of the etching holes are enlarged, and their density is significantly increased. From these experimental observations, it can be concluded that PEC etching exhibits a selectivity to etch In_xGaN/In_yGaN SSLs with a relatively higher n-type concentration and lower resistivity. The higher n-type doping allows faster etching, possibly due to the higher conductivity and greater ease of separation of photogenerated electrons and holes.

The etching evolution of the NR morphologies was further investigated by increasing the etching time. An SEM image of sample B after 30-min PEC etching at 2.2M KOH is shown in Fig. 4(a). In contrast with the 10-min PEC etching shown in Fig. 3, it is very clear to see that high-density NRs are formed underneath the whole 5-μm-diameter disk after the 30-min PEC etching. We can see that the NRs sandwiched by GaN layers are well separated. Although the PEC etching achieves well-separated NRs, it can be observed that all the NRs have an inverted conical structure on top of the In_xGaN/In_yGaN SSL, as shown in the zoomed-in SEM image inset in Fig. 4(a). This phenomenon has been previously explained by the etching selectivity of GaN faces.[34,35] Because the crystallographic components of the N-face are stronger than those of the Ga-face (0001) GaN, cones with hexagonal pyramid

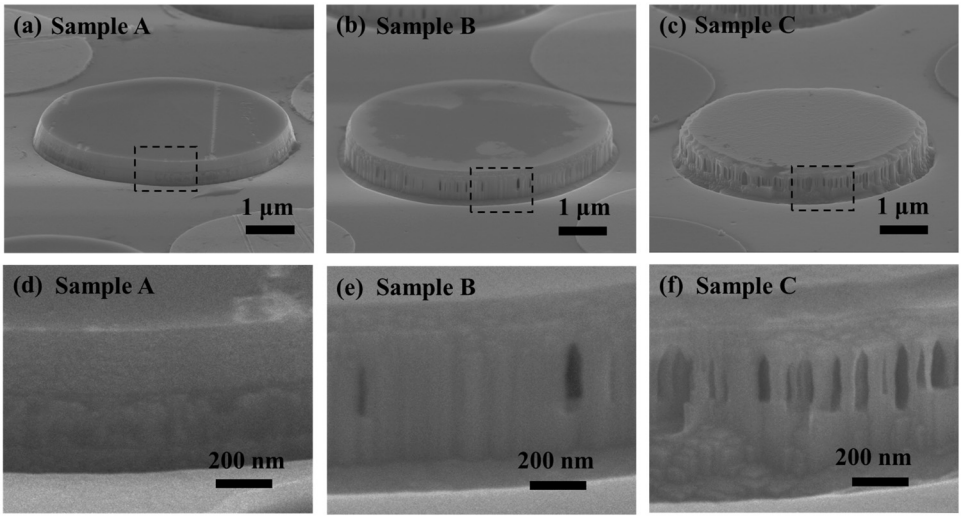

FIG. 3. Scanning electron micrograph images of (a) sample A, (b) sample B, and (c) sample C after a 10-min PEC etching in 2.2M KOH. (d)–(f) are the zoomed-in view of the area labeled by the dashed square in (a)–(c).

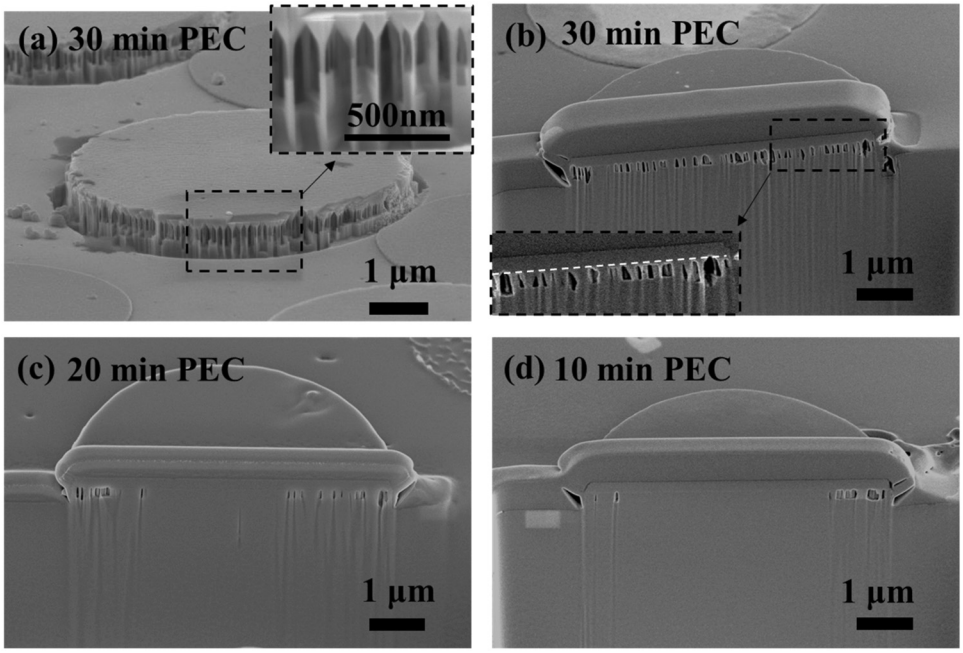

FIG. 4. Scanning electron micrograph image of sample B etched by 30-min PEC etching at 2.2M KOH; the inset: zoomed-in view of the region in the dashed square. (b)–(d) Scanning electron micrograph images of a cross section along the diameter of the disk prepared by FIB for sample B etched by PEC etching at 2.2M KOH for (a) 30, (b) 20, and (c) 10 min.

structures will be produced during etching. The NR formation is determined by selective PEC etching of n-type In_xGaN/In_yGaN SSLs. However, due to the relatively large amount of etchant at the edges of the disk, the etching selectivity of the GaN faces is comparable to the bandgap selectivity. Due to this phenomenon, cones with pyramidal shapes are formed at the edges of the disk.

In addition to investigating the NR formation under the disk other than at its edges, the NRs under the disk were exposed using FIB to cut the disk along its diameter. A strip of Pt with a 0.5-μm thickness was used to protect the disk. SEM images of sample B after PEC etching of 30, 20, and 10 min are shown in Figs. 4(b), 4(c), and 4(d), respectively. Compared with the NRs at the edges of the disk, the height of the hexagonal pyramids on top of the NRs located in the center regions is decreased. This is attributed to the lower concentration of the etchant in the center region than at the edge regions, which makes light-induced selective PEC etching dominate the process. Furthermore, it is evident that both the NR density and the lateral etching depth increase with time as etching proceeds. It should be noted that PEC etching time longer than 30 min could obtain more uniform NRs but possibly chemical etch the top GaN layer. The lateral etch depth was observed to be 0.6–1.1 μm for 10 min and 1.2–1.8 μm for 20 min. With an etching time of 30 min, the n-type In_xGaN/In_yGaN SSLs were completely etched into well-separated NRs with diameters in the range of 25–80 nm. The lateral selective etching rate of the In_xGaN/In_yGaN SSLs was calculated to be 60–110 nm/min by dividing the NR formation distance from the edge to the center of the disk over the etching time. In addition, the areal density of the NRs along the cross section was counted to be in the range of 7×10^8 to 1×10^9 cm^{-2}, which is comparable with the threading dislocation density (TDD) of 3×10^9 cm^{-2} for sample B. The TDD is calculated from the ω-scan full width at half maximum (FWHM) results of high-resolution X-ray diffraction. It is well known that the lattice mismatch between GaN and sapphire generates high-density threading dislocations. These threading dislocations start from the interface between GaN and the sapphire substrate and subsequently propagate to the GaN surface if not absorbed. The zoomed-in SEM image in Fig. 4(b) clearly shows that the top GaN layer was well protected without etching. The white dashed line labeling the AlGaN layer position confirms that AlGaN functions as a barrier layer blocking the electron transfer, which prevents the etching reaching GaN.

The effect of KOH concentration on the PEC etching has been studied using different KOH concentrations. To examine the 20 min PEC etching of sample B in 2.2M KOH [Fig. 4(e)], concentrations of 0.55, 0.14, and 0.04M KOH were used, as shown in Figs. 5(a)–5(c), respectively. It is apparent that both the NR density and lateral etching depth increased when the KOH concentration decreased from 2.2 to 0.55M. It should be noted that NR formation is an etching process combining light-assisted PEC etching and crystallographic chemical etching without light assistance. The PEC etching is mainly dependent on the holes participating in the surface oxidation of N-polar InGaN. With a lower KOH concentration of 0.14M, the disk was etched into a mushroom structure, with an undercut structure instead of a well-separated NR structure, as shown in Fig. 5(b). In this situation, crystallographic chemical etching without light assistance is comparable to light-induced selective PEC etching, with the suppressed bandgap selectivity etching inducing the partial etching of the GaN membrane on top. Figure 5(c) shows that only some of the edge regions were etched by 0.04M KOH. It can be concluded that etching in KOH solutions with concentrations lower than 0.04M confines the reaction kinetics and leads to a low etching rate. These results suggest that the KOH concentration is an influential factor for PEC etching.

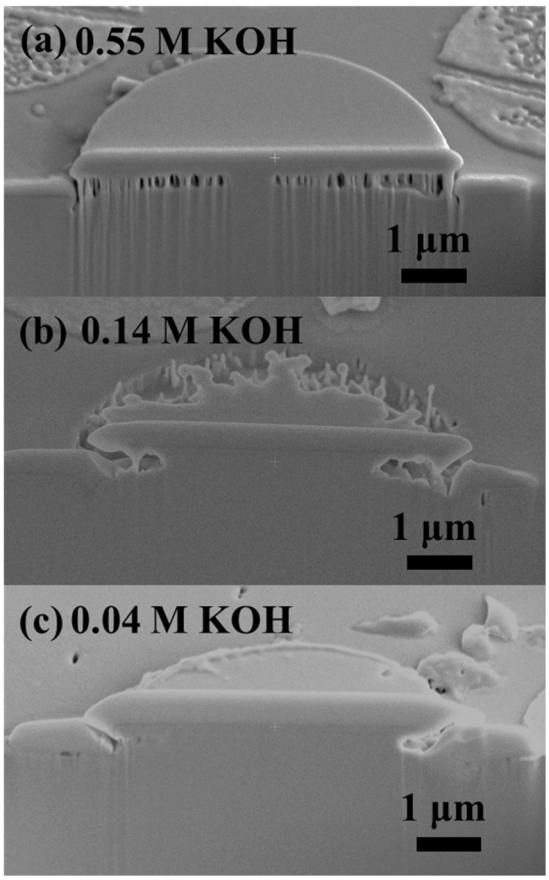

FIG. 5. SEM images of the cross section along the diameter of the disk prepared by FIB of sample B etched by 20 min PEC etching at KOH concentrations of (a) 0.55M, (b) 0.14M, and (c) 0.04M.

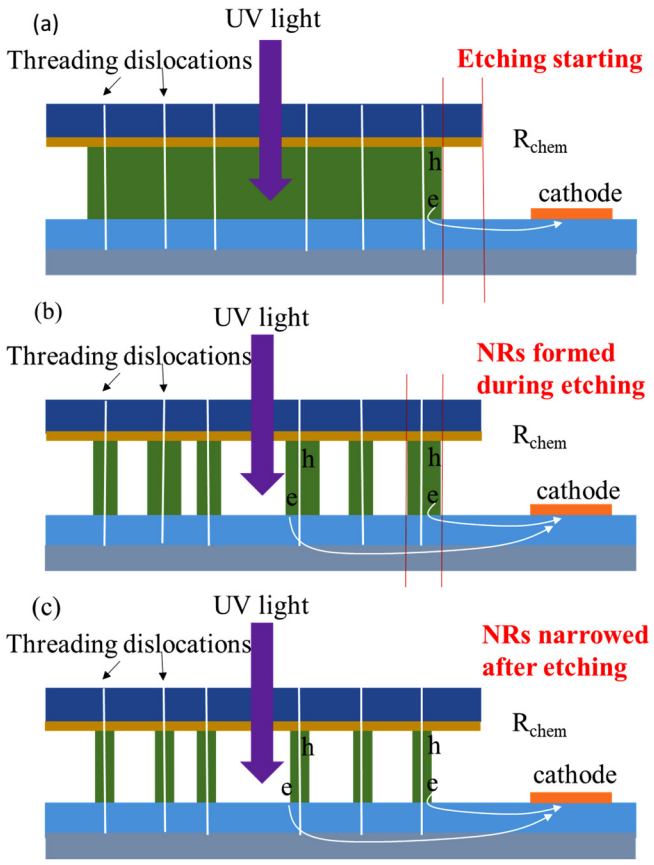

FIG. 6. Schematic process diagram for the etching mechanism of PEC. (a) Electron-hole pairs created by the light and selective lateral etching of SSLs starting. (b) Well-separated NRs formed. (c) NRs narrowing to the small size.

The etching mechanism of the well-separated NRs is illustrated in Fig. 6. The PEC etching process of the InGaN NRs was carried out in an electrochemical cell where the InGaN material to be etched acts as the anode and a Ti/Au electrode acts as the cathode. When the InGaN semiconductor material is in contact with KOH electrolyte, a depletion region in the material is created near the semiconductor-electrolyte interface, causing upward band bending. First, electron-hole pairs are created by the photons in the n-type In_xGaN/In_yGaN SSLs. Second, the electrons are extracted through the cathode, while the holes are accelerated toward the InGaN-electrolyte interface by the curvature of the band bending. The presence of photogenerated holes at the InGaN-electrolyte interface allows the ionic dissolution of the In_xGaN/In_yGaN SSLs, which are oxidized by the holes and then become etchable in KOH, which leads to the etching shown in Fig. 6(a). Considering the lamp power is fixed to get the same light intensities, the etching rate (R_{chem}) depends on three main factors: the recombination rate of the electron and hole pairs (R_{recomb}), the rate of holes diffusing to the In_xGaN/In_yGaN SSL surface (R_{dif}), and the rate of holes being trapped by threading dislocation (R_{dis}). The large R_{dif} means a large number of holes contribute to the etching. PEC etching is highly sensitive to the threading dislocations. The presence of ionized charges at dislocations may effectively reduce the concentration of holes available for the etching reaction. As the etching surface approaches the threading dislocations, the probability that holes will be captured by these dislocations (R_{dis}) increases,[36,37] leading to a vicinity of the threading dislocations that will not be etched as well as the formation of the NR structure, as shown in Fig. 6(b). This is also consistent with other PEC etching studies of GaN, which point out that materials with a low dislocation density have a higher etching rate than highly dislocated materials.[38] These electrically inactive dislocations can be broken off by solution agitation during stirring and/or sonication.[39] It needs to be noted that GaN having a high TDD is due to the shortness of both the lattice parameter and thermal expansion coefficient-matched substrate, and dislocation-induced NRs can be etched away using a lamp with a high light intensity.[40] Furthermore, when narrow NRs are formed, as shown in Fig. 6(c), it is difficult for PEC etching to separate electrons and holes effectively due to the nonradiative

recombination occurring at the dislocations. As the NRs reach a critical diameter, where they are mostly depleted and R_{recomb} has substantial competition with R_{dis}, crystallographic chemical etching without light assistance will be dominant. Ultimately, high-density and well-separated NRs will be formed. This NR structure can be used in future LEDs to improve the light extraction efficiency via light scattering around the NRs.

IV. SUMMARY AND CONCLUSIONS

This paper reports, for the first time, selective lateral etching of both well-vertically aligned and well-separated InGaN NR arrays sandwiched by GaN layers using the method of selective PEC etching. The mechanism of the etching of the well-separated InGaN NRs has also been systematically demonstrated. The In_xGaN/In_yGaN SSL etching evolution was enhanced with an increased n-type concentration of the InGaN SSLs. It was also confirmed that the structure of the NRs and the PEC lateral etching depth can be controlled by adjusting the etching time and KOH concentration. In addition, a 5-μm-diameter disk with InGaN NRs sandwiched by GaN was achieved by 30 min PEC etching. Our results provide a demonstration of vertically aligned and well-separated InGaN NRs, which have the potential to improve the performance of LEDs.

ACKNOWLEDGMENTS

This work was supported, in part, by Grant Nos. 16216017, T23-407/13N-2, 16302717, and C6013-16E from the Research Grants Council of Hong Kong. The authors would like to acknowledge the MCPF and NFF of HKUST for technical support. Helpful discussions with Evelyn Hu are also acknowledged.

REFERENCES

[1]S. Pimputkar, J. S. Speck, S. P. DenBaars, and S. Nakamura, Nat. Photonics **3**, 180 (2009).
[2]C. Y. Zhao, C. W. Tang, B. Lai, G. H. Cheng, J. N. Wang, and K. M. Lau, Photon. Res. **8**, 750 (2020).
[3]A. David, T. Fujii, R. Sharma, K. McGroddy, S. Nakamura, S. P. DenBaars, E. L. Hu, C. Weisbuch, and H. Benisty, Appl. Phys. Lett. **88**, 061124 (2006).
[4]Y. W. Cheng *et al.*, Nanotechnology **20**, 035202 (2009).
[5]J. J. Wierer, Jr., A. David, and M. M. Megens, Nat. Photonics **3**, 163 (2009).
[6]K. Choi, M. Arita, and Y. Arakawa, J. Cryst. Growth **357**, 58 (2012).
[7]S. D. Hersee, X. Sun, and X. Wang, Nano Lett. **6**, 1808 (2006).
[8]T. W. George, A. A. Talin, J. W. Donald, J. R. Creighton, L. Elaine, J. A. Richard, and A. Ilke, Nanotechnology **17**, 5773 (2006).
[9]C. B. Maliakkal, N. Hatui, R. D. Bapat, B. A. Chalke, A. A. Rahman, and A. Bhattacharya, Nano Lett. **16**, 7632 (2016).
[10]R. Koester, J. S. Hwang, C. Durand, D. L. S. Dang, and J. Eymery, Nanotechnology **21**, 015602 (2010).
[11]F. Schuster, F. Furtmayr, R. Zamani, C. Magén, J. R. Morante, J. Arbiol, J. A. Garrido, and M. Stutzmann, Nano Lett. **12**, 2199 (2012).
[12]V. Consonni, M. Knelangen, U. Jahn, A. Trampert, L. Geelhaar, and H. Riechert, Appl. Phys. Lett. **95**, 241910 (2009).
[13]A. Jordi *et al.*, Nanotechnology **20**, 145704 (2009).
[14]A. Liudi Mulyo, Y. Konno, J. S. Nilsen, A. T. J. van Helvoort, B.-O. Fimland, H. Weman, and K. Kishino, J. Cryst. Growth **480**, 67 (2017).
[15]D. Tham, C. Y. Nam, and J. E. Fischer, Adv. Funct. Mater. **16**, 1197 (2006).
[16]D. Paramanik *et al.*, J. Vac. Sci. Technol. B **30**, 052202 (2012).
[17]C. Y. Wang, L. Y. Chen, C. P. Chen, Y. W. Cheng, M. Y. Ke, M. Y. Hsieh, H. M. Wu, L. H. Peng, and J. Huang, Opt. Express **16**, 10549 (2008).
[18]X. Xu, Q. Wang, C. Li, Z. Ji, M. Xu, H. Yang, and X. Xu, J. Lumin. **203**, 216 (2018).
[19]E. D. Le Boulbar, C. J. Lewins, D. W. E. Allsopp, C. R. Bowen, and P. A. Shields, Microelectron. Eng. **153**, 132 (2016).
[20]Q. Li *et al.*, Opt. Express **19**, 25528 (2011).
[21]Y. Y. Lai, S. C. Hsu, H. S. Chang, Y. S. Wu, C. H. Chen, L. Y. Chen, and Y. J. Cheng, Res. Chem. Intermediat. **43**, 3563 (2017).
[22]S. Liu, C. Li, J. J. Figiel, S. R. J. Brueck, I. Brener, and G. T. Wang, Nanoscale **7**, 9581 (2015).
[23]S. P. R. M, H. Park, S. M. Kim, S. H. Jang, and J. S. Jang, J. Mater. Chem. C **3**, 8873 (2015).
[24]M. J. Schwab, D. Chen, J. Han, and L. D. Pfefferle, J. Phys. Chem. C **117**, 16890 (2013).
[25]Y. Yue, X. Yan, W. Li, H. G. Xing, D. Jena, and P. Fay, J. Vac. Sci. Technol. B **32**, 061201 (2014).
[26]R. Debnath, J. Y. Ha, B. Wen, D. Paramanik, A. Motayed, M. R. King, and A. V. Davydov, J. Vac. Sci. Technol. B **32**, 021204 (2014).
[27]Y. Jung, K. H. Baik, M. A. Mastro, J. K. Hite, C. R. Eddy, and J. Kim, Phys. Chem. Chem. Phys. **16**, 15780 (2014).
[28]L. Lu *et al.*, J. Appl. Phys. **104**, 123525 (2008).
[29]M. S. Minsky, M. White, and E. L. Hu, Appl. Phys. Lett. **68**, 1531 (1996).
[30]A. R. Stonas, P. Kozodoy, H. Marchand, P. Fini, S. P. DenBaars, U. K. Mishra, and E. L. Hu, Appl. Phys. Lett. **77**, 2610 (2000).
[31]R. Sharma, Y. S. Choi, C. F. Wang, A. David, C. Weisbuch, S. Nakamura, and E. L. Hu, Appl. Phys. Lett. **91**, 211108 (2007).
[32]C. Youtsey *et al.*, Phys. Status Solidi B **254**, 1600774 (2017).
[33]D. Wang, T. Zhu, R. A. Oliver, and E. L. Hu, Opt. Lett. **43**, 799 (2018).
[34]A. R. Stonas, T. Margalith, S. P. DenBaars, L. A. Coldren, and E. L. Hu, Appl. Phys. Lett. **78**, 1945 (2001).
[35]G. Yan, F. Tetsuo, S. Rajat, F. Kenji, P. D. Steven, N. Shuji, and L. H. Evelyn, Jpn. J. Appl. Phys. **43**, L637 (2004).
[36]T. J. Puchtler, A. Woolf, T. Zhu, D. Gachet, E. L. Hu, and R. A. Oliver, ACS Photonics **2**, 137 (2015).
[37]C. Youtsey, L. T. Romano, and I. Adesida, Appl. Phys. Lett. **73**, 797 (1998).
[38]Y. Gao, M. D. Craven, J. S. Speck, S. P. D. Baars, and E. L. Hu, Appl. Phys. Lett. **84**, 3322 (2004).
[39]J. A. Bardwell, J. B. Webb, H. Tang, J. Fraser, and S. Moisa, J. Appl. Phys. **89**, 4142 (2001).
[40]C. Youtsey, I. Adesida, L. T. Romano, and G. Bulman, Appl. Phys. Lett. **72**, 560 (1998).